LISA Astrophysics Working Group Meeting, MPA, Nov 2024

Identifying eccentric black hole mergers in dynamical formation environments

Kai Hendriks

Niels Bohr Institute, University of Copenhagen

Supervised by Johan Samsing

VILLUM FONDEN

Motivation: different formation channels

Isolated formation

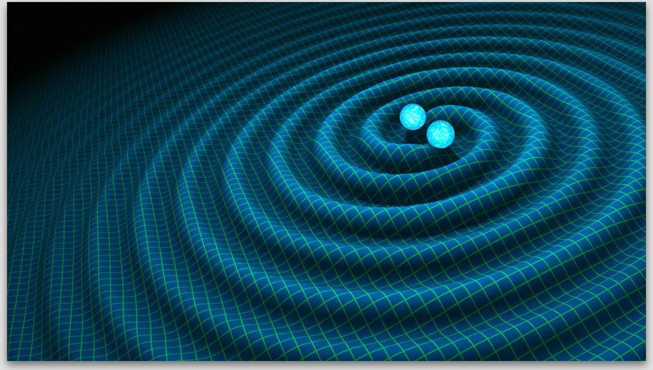

Dynamical formation

Globular clusters

Active galactic nuclei

Motivation: the dynamical channel

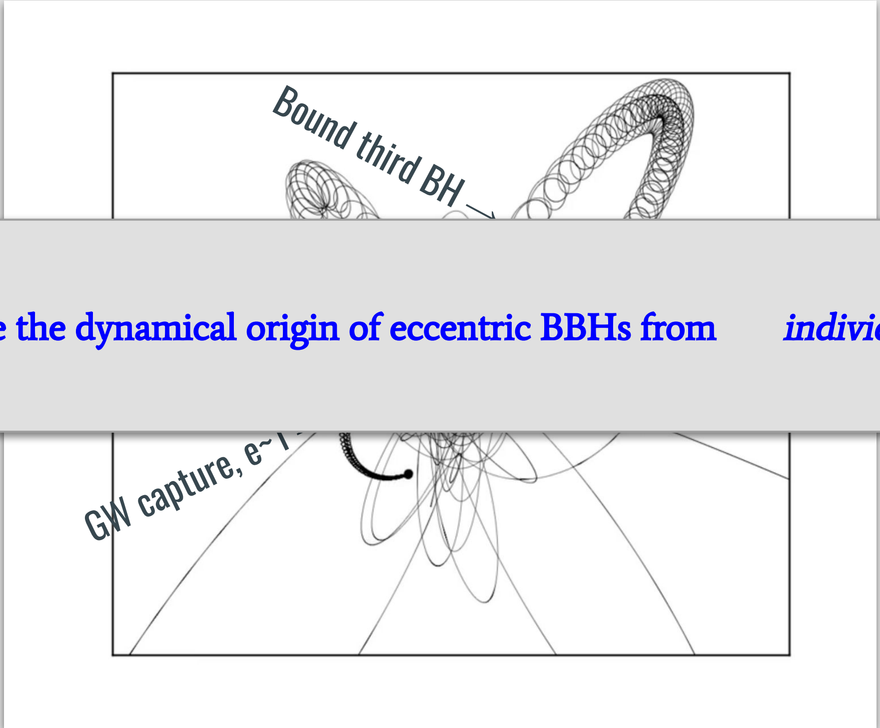

How can we probe the dynamical origin of eccentric BBHs from *individual* GW events?

Fig. 1: example of a 3-body scattering.

Setup

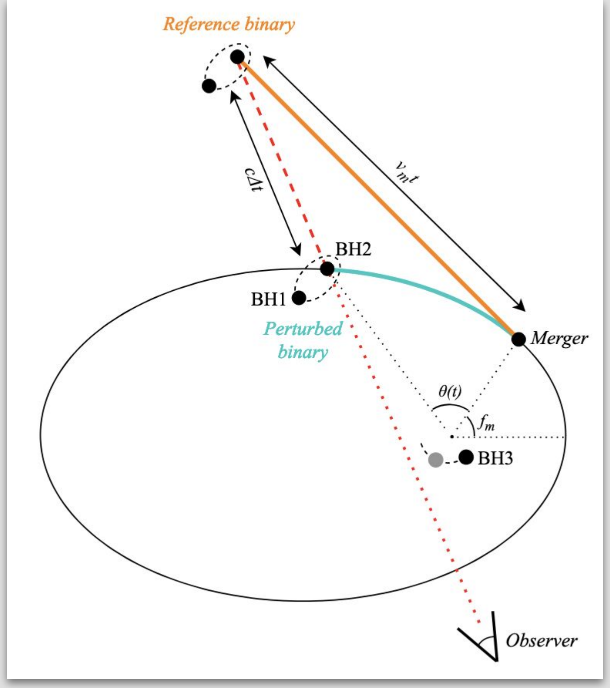

Fig. 2: setup of our system of interest.

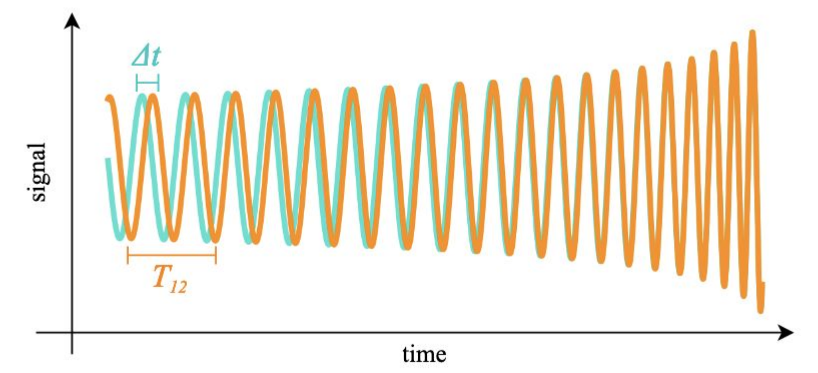

Fig. 3: perturbed waveform due to Rømer delay.

$$d\phi \approx 2\pi \frac{\Delta t(t)}{T_{12}(t)}$$

Phase shift

$$\Delta\phi(e) \approx \frac{288\sqrt{2}}{85^2 g(1)^{13/2}} \frac{c^9}{G^{9/2}} \times \frac{m_3}{R^2} \frac{r_0^{13/2}}{m_1^2 m_2^2 m_{12}^{3/2}} \times e^{78/19}(1-e^2)^{1/2} g(e)^{13/2}$$

Phase shift peaks when e~0.95!

How high can the phase shift get?

Take your favourite few-body simulation code

Simulate many binary-single interactions typical for clusters

Calculate the phase shift for those in triple configuration

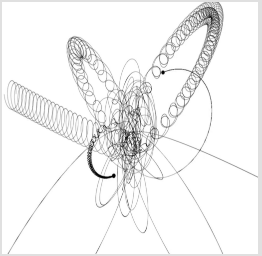

How high can the phase shift get?

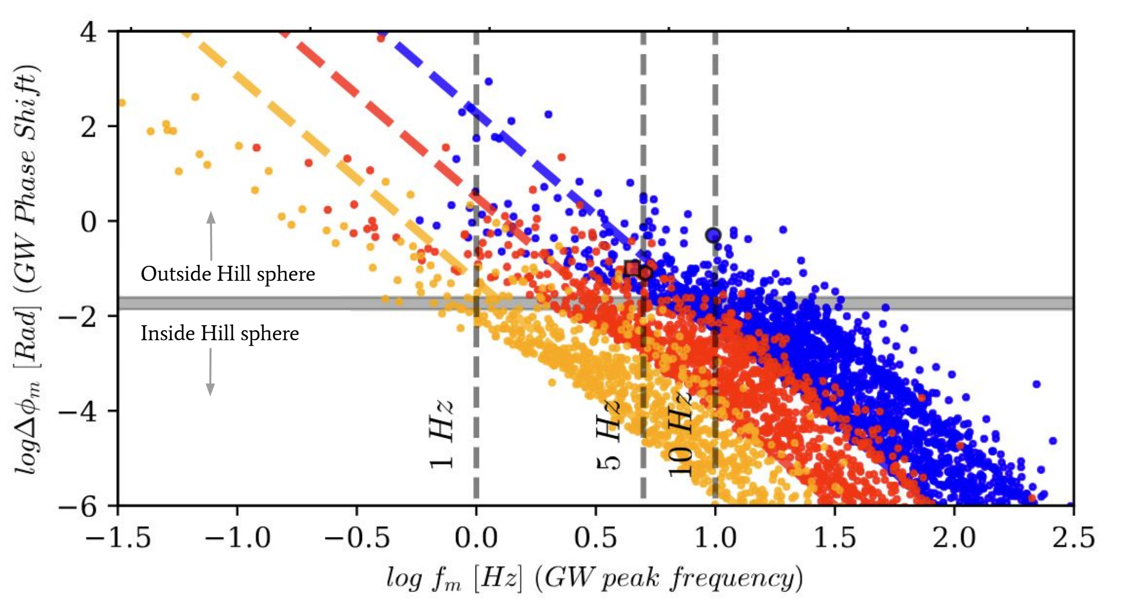

Fig. 4: maximum phase shift as a function of the peak GW frequency at formation of the binary. We use an equal mass triple of 20 solar masses. The different colours represent different initial semi-major axes: from 0.01 AU (blue) to 0.1 AU (red) and 1 AU (orange). The horizontal lines are the astrophysically expected upper limits.

Summary

How can we probe the dynamical origin of eccentric BBHs from *individual* GW events?

GW phase shift!

Can map the environment in which the binary formed

3G detectors such as LISA/ET/CE may be able to detect this environmental effect

Questions?

2408.04603

Contact me at kai.hendriks@nbi.ku.dk!

Astrophysical scenarios: 3-body scatterings

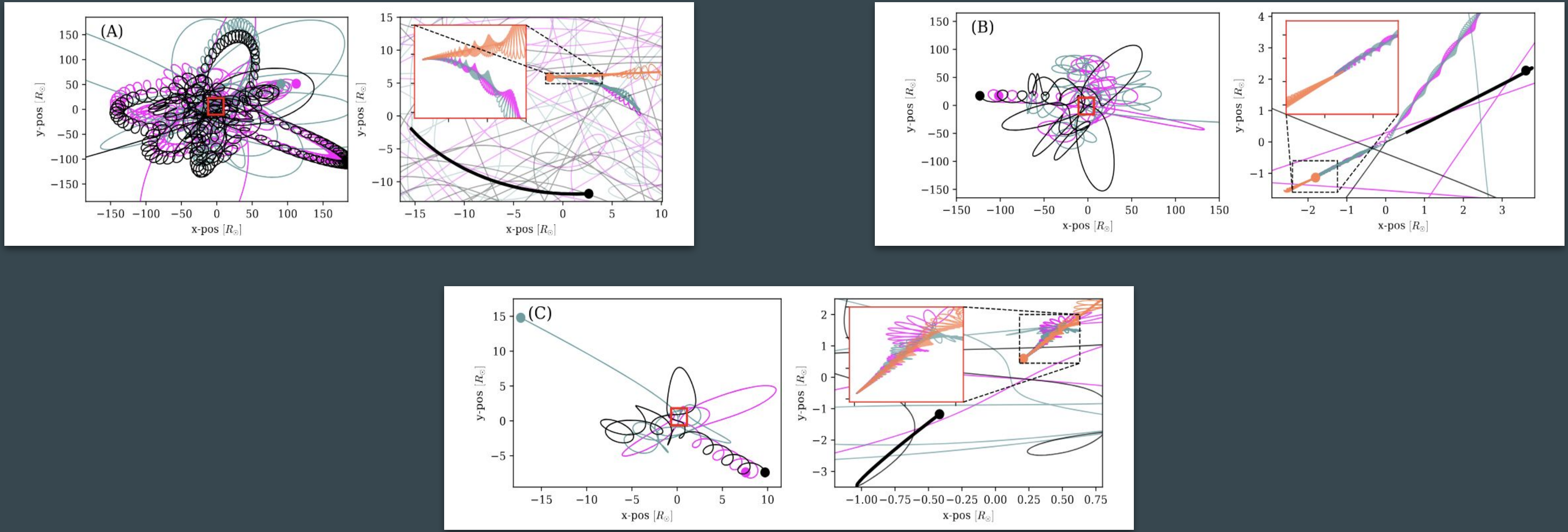

Fig. 13: examples of 3-body scatterings that lead to phase shifts higher than the theoretical maximum.

Astrophysical scenario: 3-body scatterings

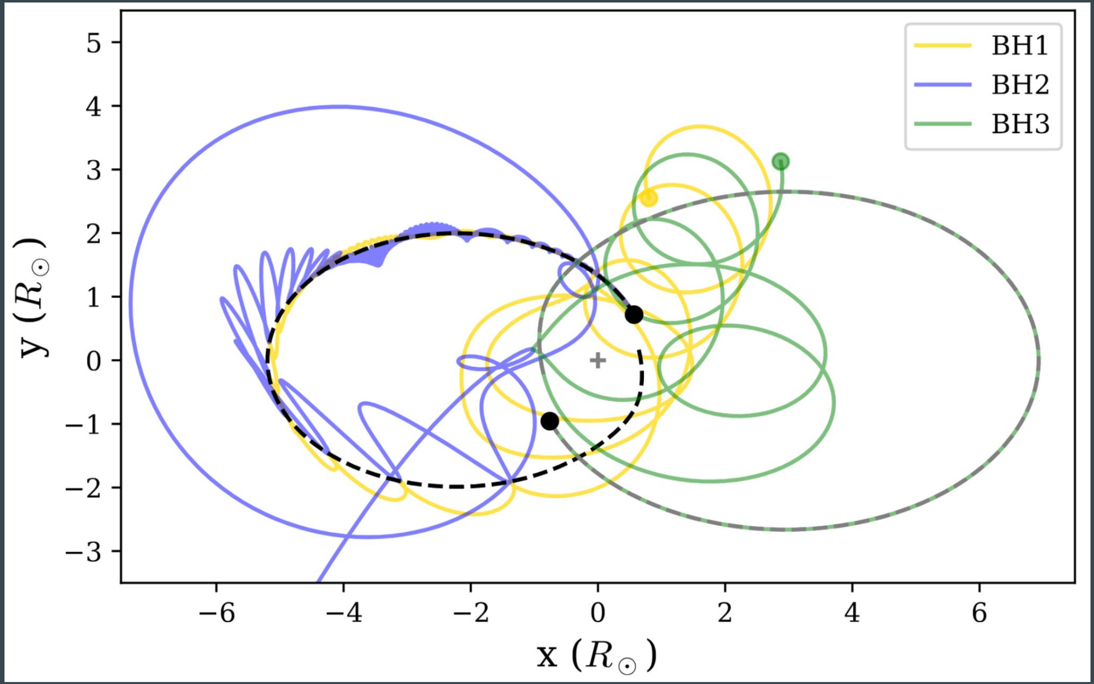

Fig. 8: 3-body scattering (5, 15 and 15 Msun) resulting in an inspiralling and merging binary on a bound orbit around a third object.

Astrophysical scenario: 3-body scatterings

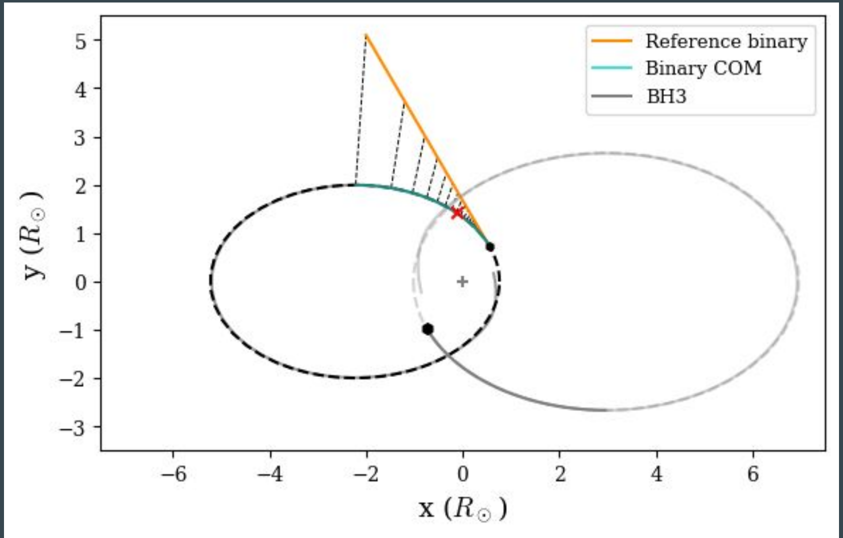

Fig. 9: binary COM, reference trajectory and perturber trajectory of the scattering in question. We can extract the Rømer delay and phase shift from this.

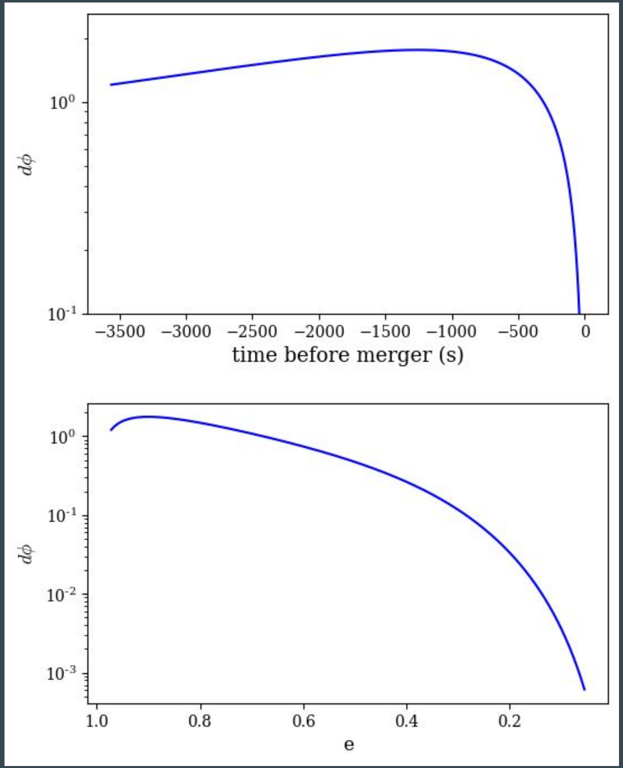

Fig. 10: phase shift of this scattering, as a function of time (top) and binary eccentricity (bottom).

Phase shift: eccentric outer orbit

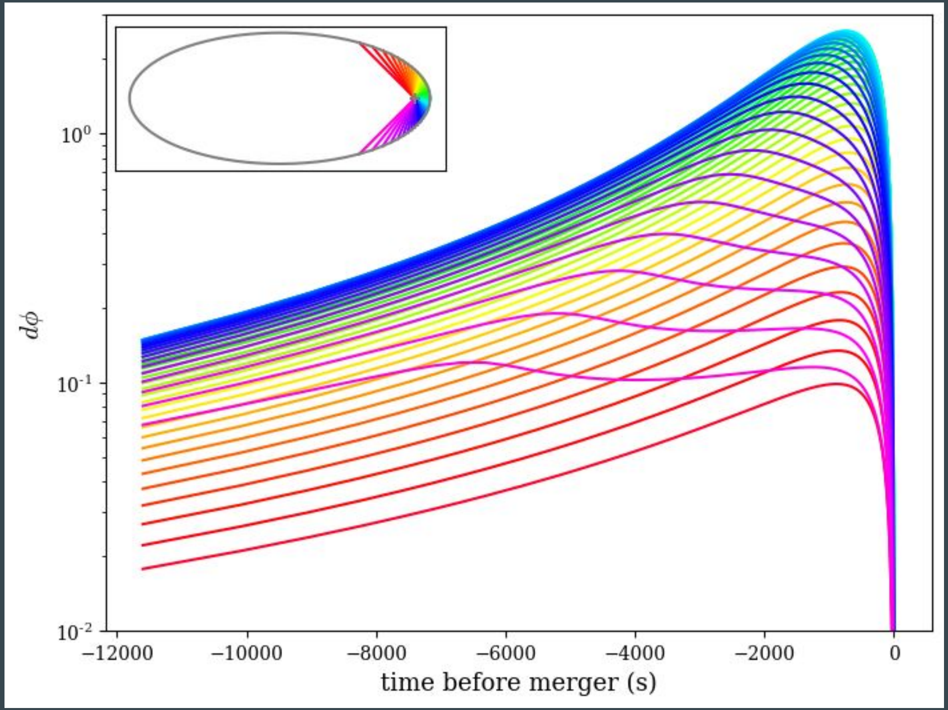

Fig. 7: phase shift as a function of time, for different realisations of f_m, ranging from -¾ π to ¾ π. We still use an eccentric 5 $M_\odot$ equal-mass binary, inspiralling on an eccentric orbit (e=0.9, a=30 $R_\odot$) around a 100 $M_\odot$ perturber. The binary assembles at a semi-major axis a_0=1.3 $R_\odot$ and e_0 = 0.9999.

Stereoscopic images

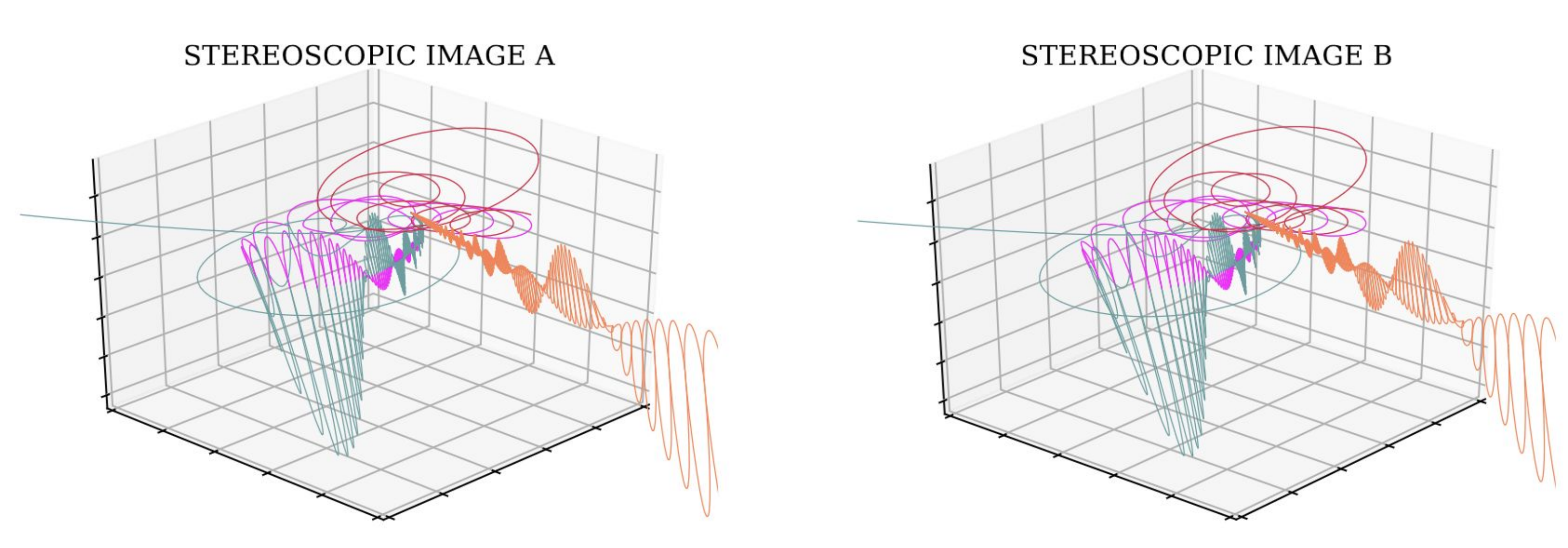

Phase shift: analytical approximation

- Problem: no analytical description when outer orbit is eccentric

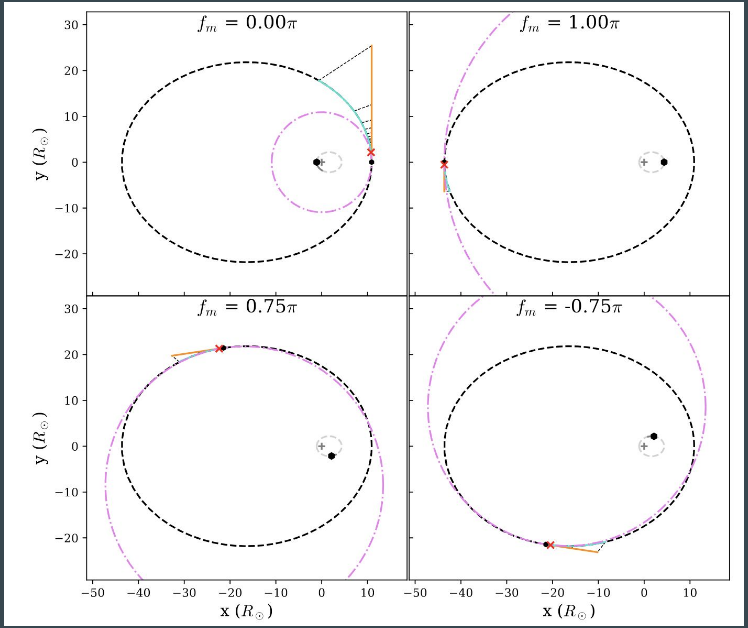

Fig. 9: trajectories and phase shift of an eccentric 5 $M_\odot$ equal-mass binary, inspiralling on an eccentric orbit (e=0.9, a=30 $R_\odot$) around a 100 $M_\odot$ perturber. The binaries assemble at a semi-major axis a_0=1.3 $R_\odot$ and e_0 = 0.9999, for 4 different outer phases at merger.

$$\Delta\phi(e) \approx \frac{288\sqrt{2}}{85^2 g(1)^{13/2}} \frac{c^9}{G^{9/2}} \times \frac{m_3}{R^2} \frac{r_0^{13/2}}{m_1^2 m_2^2 m_{12}^{3/2}} \times e^{78/19}(1-e^2)^{1/2} g(e)^{13/2}$$

Phase shift: circular outer orbit

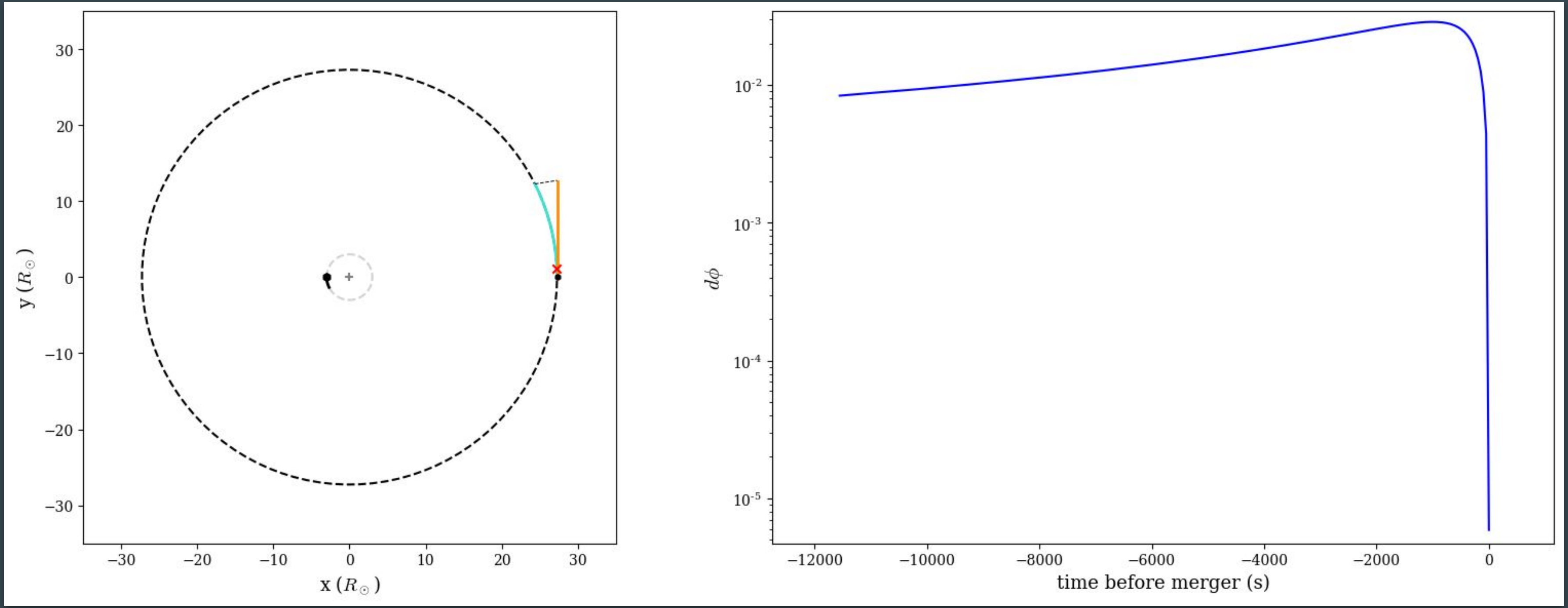

Fig. 6: trajectory and phase shift of an eccentric 5 $M_\odot$ equal-mass binary, inspiralling on a circular orbit (30 $R_\odot$) around a 100 $M_\odot$ perturber. The binary assembles at a semi-major axis a_0=1.3 $R_\odot$ and e_0 = 0.9999.

Phase shift: effect of outer eccentricity

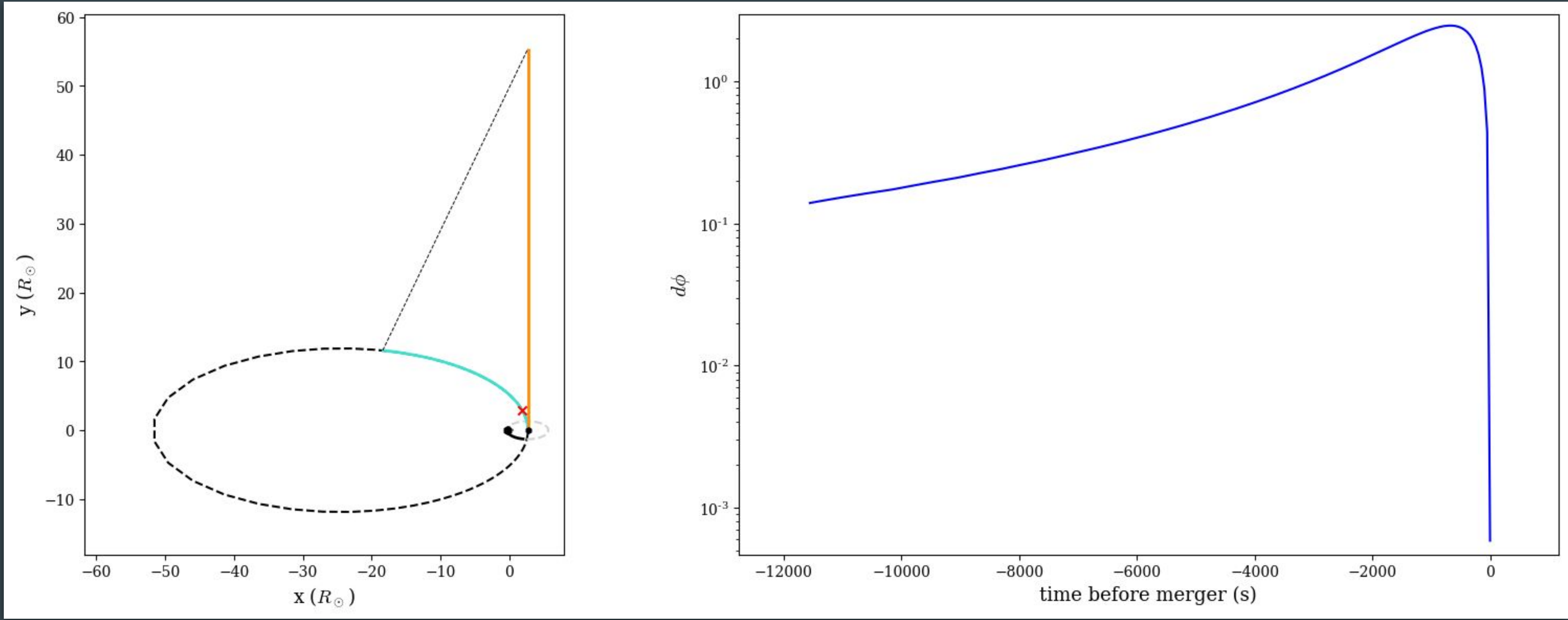

Fig. 8: trajectory and phase shift of an eccentric 5 $M_\odot$ equal-mass binary, inspiralling on an eccentric orbit (e=0.9, a=30 $R_\odot$) around a 100 $M_\odot$ perturber. The binary assembles at a semi-major axis a_0=1.3 $R_\odot$ and e_0 = 0.9999, and merges at pericentre (f_m=0).

Phase shift: eccentric outer orbit

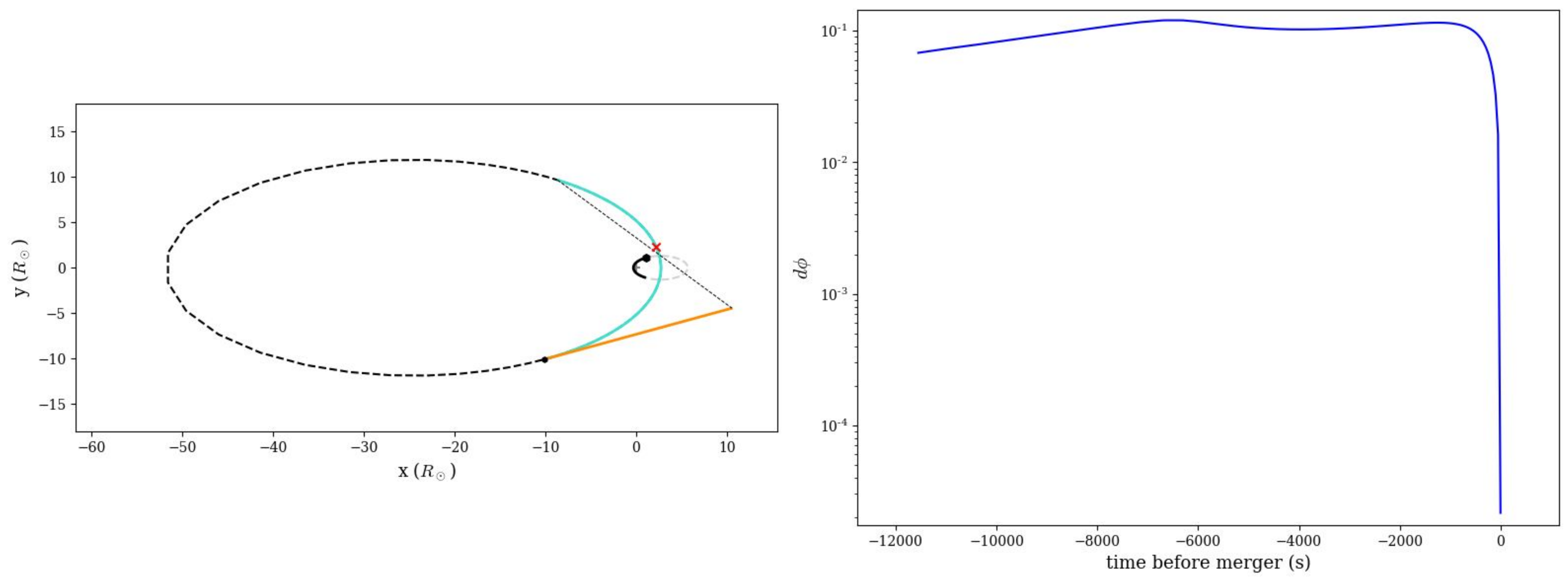

Fig. 10: trajectory and phase shift of an eccentric 5 $M_\odot$ equal-mass binary, inspiralling on an eccentric orbit (e=0.9, a=30 $R_\odot$) around a 100 $M_\odot$ perturber. The binary assembles at a semi-major axis a_0=1.3 $R_\odot$ and e_0 = 0.9999, and merges at f_m = -¾ π.

Phase shift: effect of the outer eccentricity

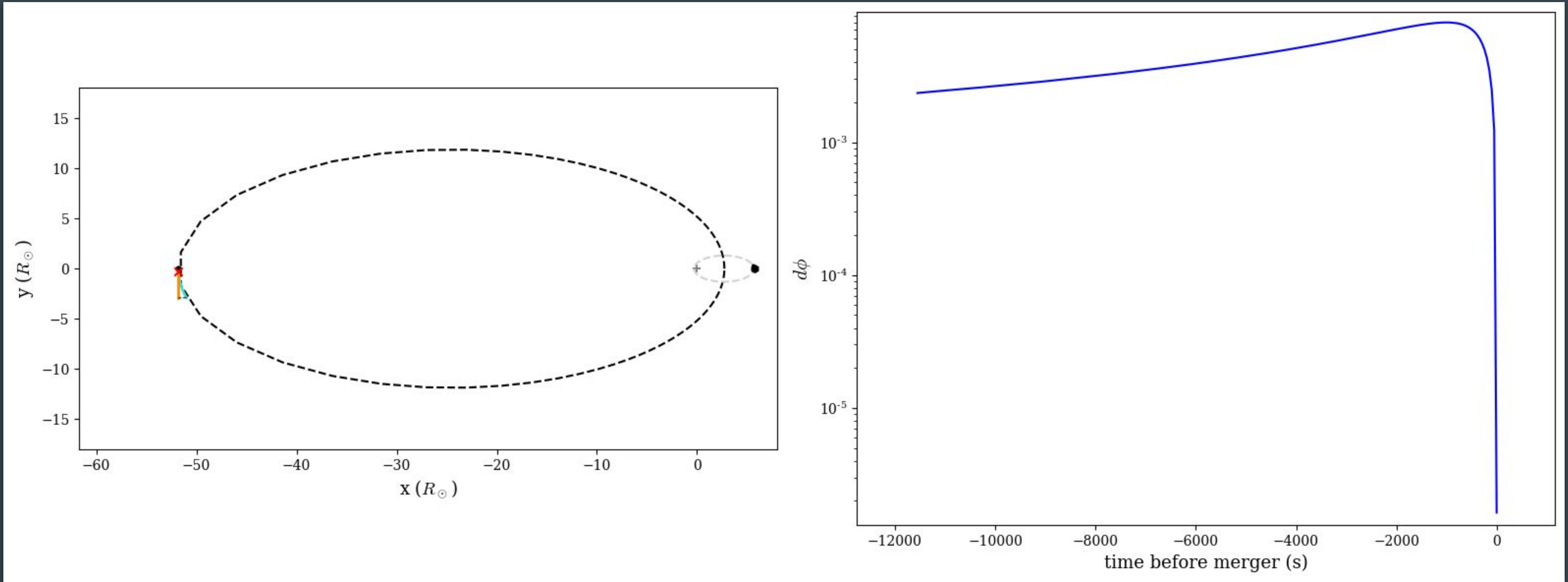

Fig. 9: trajectory and phase shift of an eccentric 5 $M_\odot$ equal-mass binary, inspiralling on an eccentric orbit (e=0.9, a=30 $R_\odot$) around a 100 $M_\odot$ perturber. The binary assembles at a semi-major axis a_0=1.3 $R_\odot$ and e_0 = 0.9999, and merges at apocentre ($f_m = \pi$).

Astrophysical scenario: 3-body scatterings

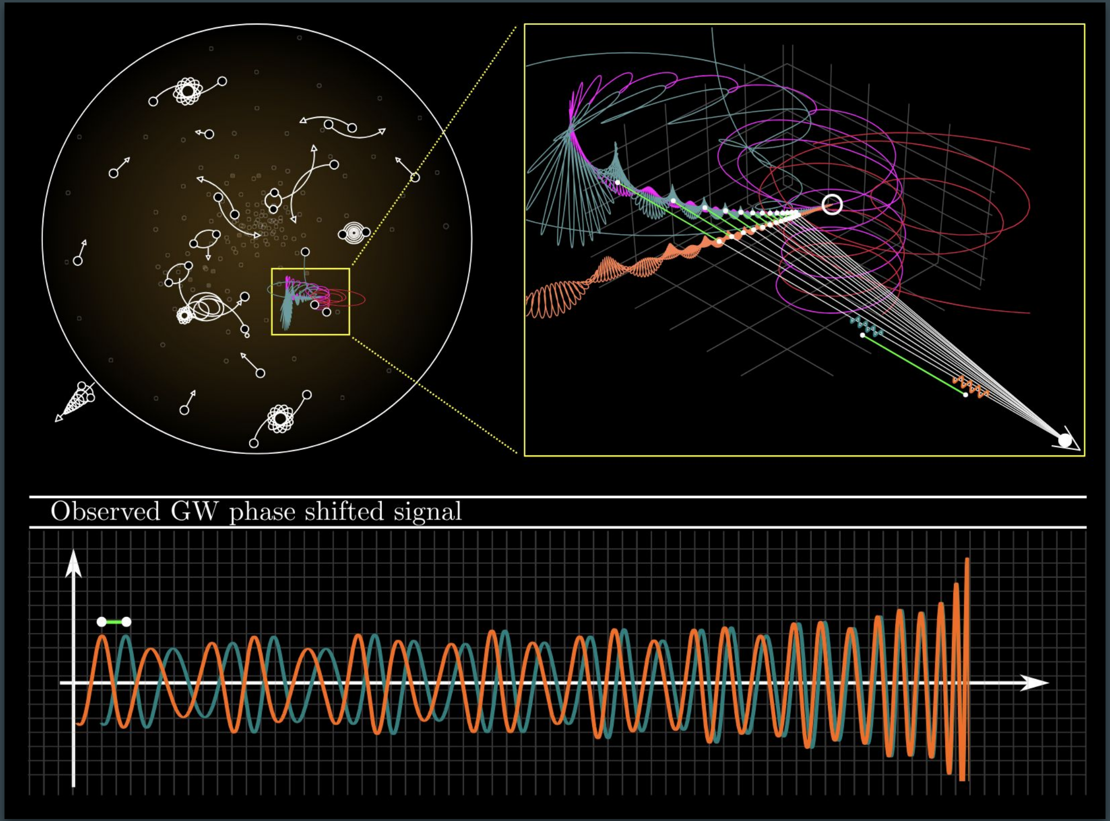

Fig. 11: 3-body scatterings with GW mergers in a stellar cluster..